RSC Advances

PAPER

View Article Online
View Journal | View Issue

Cite this: *RSC Adv.*, 2019, **9**, 16305

Cu(II)/Ni(II)–organic frameworks constructed from the homometallic clusters by 5-(2-carboxyphenoxy)isophthalic acid and N-ligand: synthesis, structures and visible light-driven photocatalytic properties†

Qi-Wei Xu, Qiu-Shuang Wang, Shan-Shan Li and Xia Li *

Four new complexes, namely, Cu_2(O-cpia)$(btb)_{0.5}\cdot(OH)$ (**1**), Cu_3(O-cpia)$_2(bpy)_2$ (**2**), $[Ni_2$(O-cpia)(phen)$\cdot(OH)\cdot H_2O]\cdot 2H_2O$ (**3**) and $[Ni_3$(O-cpia)$_2(bpy)_3\cdot 2H_2O]\cdot 2H_2O$ (**4**) (O-cpia = 5-(2-carboxyphenoxy)isophthalic acid, btb = 1,4-bis(1,2,4-triazol-1-yl)butane, bpy = 4,4′-bipyridine) were successfully isolated under hydrothermal conditions. The four complexes exhibit different architectures constructed from different homometallic clusters varying from mononuclear, binuclear to tetranuclear metal(II) polyhedra as Second Building Blocks (SBUs). **1** features a 3D framework constructed from the tetranuclear clusters $[Cu_4(\mu_3\text{-}OH)_2]$ as SBUs, linked with $Cu(1)O_4N$ and $Cu(2)O_5$ polyhedra by O-cpia/btb mixed linkers. **2** also exhibits a 3D structure based on trinuclear clusters $[Cu_3(COO)_4]$ SBUs, bridged with $Cu(1)O_3N_2$ and $Cu(2)O_4$ polyhedra *via* O-cpia/bpy mixed ligands. **3** shows a 2D network consisting of tetranuclear clusters $[Ni_4(\mu_3\text{-}OH)_2]$ SBUs, which are bridged with $Ni(1)O_4N_2$ and $Ni(2)O_6$ through O-cpia ligands. It is worth noting that **4**, with a 3D structure, is generated from the binuclear clusters $[Ni_2(COO)_4]$ ($Ni(1)O_4N$) and mononuclear metal Ni(2) cores ($Ni(2)O_4N_2$) as SBUs, and bridged by O-cpia/bpy mixed ligands. Meanwhile, the degradation of dyes (RhB) by the complexes under visible light irradiation was studied. **1–4** are semiconducting in nature, with E_g of 1.30 eV (**1**), 1.78 eV (**2**), 2.85 eV (**3**) and 2.14 eV (**4**). Cu(II) complexes **1** and **2** are highly efficient photocatalysts for the degradation of RhB under visible light irradiation.

Received 28th February 2019
Accepted 14th May 2019

DOI: 10.1039/c9ra01496a

rsc.li/rsc-advances

Introduction

Metal–organic frameworks (MOFs) are prepared by the self-assembly of metal ions or clusters with organic ligands. A variety of structural types have been reported, such as one-, two- and three- dimensional structures, which are based on M–O–M, homometallic clusters as Second Building Blocks (SBUs).[1–4] MOFs, with interesting architectures, also have good physico-chemical properties, which can be potentially applied to many fields such as catalysis, luminescence, gas adsorption, magnetic materials, *etc.*[3,5–10] In the past few decades, MOFs have attracted wide attention. Transition metal cations have various coordination geometries which can be used in various crystal architectures.[6,11,12] For example, Zn(II), Cd(II), Cu(II), Ni(II), and Co(II), with different electron configurations and coordination numbers, may form compounds in various architectures, which can be applied to catalysis and luminescence.[13–18] Among them, Cu(II) and Ni(II) complexes have shown to be effective chemical photocatalysts under visible light irradiation.[19–22] The development of MOFs has provided more opportunities for new photocatalysts, because of their diverse structures containing variable valence electrons and empty orbits of the metal center, high thermal and chemical stability.[23,24] Recently, MOFs have been demonstrated with a good photocatalytic activity for the degradation of organic dyes such as methyl orange, methylene blue and rhodamine B (RhB) under visible light irradiation.[15,19,25–29] Due to the high importance of environment protection, how to effectively remove organic pollutants has become a hot social issue, leading to high demands for high-efficiency photocatalysts.

We are interested in synthesizing new MOFs with diverse structures, and in studying their photocatalytic properties. Metal polyhedra in hybrid frameworks with polycarboxylate ligands and N-ligands have led to numerous examples of MOFs materials with interesting structures and remarkable physical properties. This has promotes the synthesis of new MOFs using a tricarboxylate ligand with N-donor co-ligands to construct new MOFs with Cu(II)/Ni(II) metal nodes and the study of their catalytic performance. 5-(2-Carboxyphenoxy)isophthalic acid ($O\text{–}H_3$cpia), semi-rigid ligand is composed of tricarboxylate groups, which has diverse binding capability as bridging ligand

Department of Chemistry, Capital Normal University, Beijing, 100048, China. E-mail: xiali@cnu.edu.cn; Fax: +86 1068902320; Tel: +86 1068902320

† Electronic supplementary information (ESI) available. CCDC 1811807, 1832419, 1832425, 1832426. For ESI and crystallographic data in CIF or other electronic format see DOI: 10.1039/c9ra01496a

by multiple coordination modes, leading to interesting MOFs. Some studies have been reported regarding the synthesis and structural analysis of MOFs with O–H_3cpia.[30–33] N-donor molecules are important building blocks in crystal engineering because of their ability of coordinating to metal centres and forming networks.[34] A number of N-donor ligands have been used for the synthesis of MOFs with carboxylic acids to tune the dimensionality of the MOFs.[35,36] Phen has high affinities for metal ions and has been used to prepare complexes with excellent photophysical and chemical properties.[37,38] Neutral N-ligands, such as 4,4′-bipyridine (bpy)[39,40] and 1,4-bis(1,2,4-triazol-1-yl)butane (btb),[41,42] can pillar metal-carboxylate coordination polymer motifs into higher dimensions structures. In addition, the btb flexible ligand can adopt TTT, GTG, and GTT conformations in N4 : N4′-mode and act as a bridge between two central metal atoms to form new and unpredictable structural motifs.

Driven by the interest to synthesize new MOFs with diverse structures, and to study their photocatalytic properties, the O–H_3cpia and phen/bpy/btb ligands were introduced in the reaction system of Cu(II) and Ni(II) metal salt in H_2O solvent, and new complexes, *i.e.*, Cu_2(O-cpia)$(btb)_{0.5}\cdot(OH)$ (**1**), Cu_3(O-cpia)$_2(bpy)_2$ (**2**), $[Ni_2$(O-cpia)$(phen)\cdot(OH)\cdot H_2O]\cdot 2H_2O$ (**3**) and $[Ni_3$(O-cpia)$_2(bpy)_3\cdot 2H_2O]\cdot 2H_2O$ (**4**) were synthesized. We also studied the structures and ability of the complexes as photocatalysts for the degradation of the organic dyes RhB. Interestingly, these new compounds show different interesting architectures based on the different homometallic clusters varying from mononuclear, binuclear to tetranuclear clusters as Second Building Blocks (SBUs) by different organic linkers. The catalytic properties of the complexes to the degradation of rhodamine B (RhB) organic pollutant under visible light irradiation were studied as well. Complexes **1** and **2** are proved to be highly efficient photocatalysts for the degradation of the RhB under visible light irradiation.

Experimental

Materials and methods

All experimental materials are commercially available and could be used as received without further purification. Elemental analyses (C, H, and N) were run on an Elementar Vario EL elemental analyzer. Powder X-ray diffraction (PXRD) was carried out on a PANaytical X'Pert PRO MPD diffractometer for Cu Kα radiation (λ = 1.5406 Å). Infrared (IR) spectra were recorded on a Bruker Tensor 37 spectrophotometer using the KBr pellets in the range 4000–400 cm^{-1}. The thermogravimetric analyses (TGA) were performed on a HCT-2 thermal analyzer under air atmosphere from the temperature of 25 to 800 °C at a heating rate of 10 °C min^{-1}. Solid UV-visible spectra were obtained on a Japan Shimadzu UV-2600 spectrophotometer. UV-vis spectra were recorded on a 2550 UV-vis spectrophotometer (Shimadzu, Japan) at room temperature.

Synthetic procedures

Synthese of Cu_2(O-cpia)$(btb)_{0.5}\cdot(OH)$ (1). A mixture of $Cu(Ac)_2\cdot 2H_2O$ (0.5 mmol), 5-(2-carboxyphenoxy)isophthalic acid (0.1 mmol), 1,4-bis(1,2,4-triazol-1-yl)butane (0.1 mmol), distilled water (10 mL) and sodium hydroxide solution (0.1 mL 2 mol L^{-1}) was sealed in a 25 mL Teflon-lined stainless container, which was heated at 140 °C for 3 days. With cooling to room temperature, dark green block-shaped crystals were found, washed with distilled water, and dried in air (yield 87%, based on O–H_3cpia). Anal. calc. for $C_{19}H_{14}N_3O_8Cu_2$: C, 42.22; H, 2.59; N, 7.78%. Found (%): C, 42.34; H, 2.54; N, 7.81%. IR (KBr pellet: cm^{-1}): 3459 (m), 3078 (w), 1619 (vs), 1450 (s), 1384 (s), 1287 (m), 1257 (s), 1205 (s), 748 (s), 725 (s).

Synthese of Cu_3(O-cpia)$_2(bpy)_2$ (2). The product was the same as that for complex **1** except that 1,4-bis(1,2,4-triazol-1-yl)butane was replaced by 4,4′-bipyridine (yield 88%, based on O–H_3cpia). Anal. calc. for $C_{50}H_{30}N_4O_{14}Cu_3$: C, 54.45; H, 2.72; N, 5.08%. Found (%): C, 54.42; H, 2.74; N, 5.07%. IR (KBr pellet: cm^{-1}): 3439 (s), 3083 (w), 1611 (vs), 1588 (vs), 1412 (s), 1369 (s), 1212 (m), 814 (m), 775 (w), 723 (w).

Synthese of $[Ni_2$(O-cpia)$(phen)\cdot(OH)\cdot H_2O]\cdot 2H_2O$ (3). A mixture of $NiSO_4\cdot 6H_2O$ (0.5 mmol), 5-(2-carboxyphenoxy)isophthalic acid (0.1 mmol), 1,10-Phenanthroline monohydrate (0.1 mmol), distilled water (10 mL) and sodium hydroxide solution (0.1 mL 2 mol L^{-1}) was sealed in a 25 mL Teflon-lined stainless container, which was heated at 180 °C for 3 days. Green block-shaped crystals were found (yield 42%, based on O–H_3cpia). Anal. calc. for $C_{27}H_{22}N_2O_{11}Ni_2$: C, 48.50; H, 3.29; N, 4.19%. Found (%): C, 48.48; H, 3.27; N, 4.21%. IR (KBr pellet: cm^{-1}): 3461 (vs), 1621 (vs), 1572 (vs), 1430 (s), 1398 (s), 1255 (m), 1214 (m), 840 (m), 727 (m), 667 (s).

Synthese of $[Ni_3$(O-cpia)$_2(bpy)_3\cdot 2H_2O]\cdot 2H_2O$ (4). The product was the same as that for complex **3** except that 1,10-phenanthroline monohydrate was replaced by 4,4′-bipyridine. That was heated at 160 °C for 3 days. Block-shaped crystals were found (yield 47%, based on O–H_3cpia). Anal. calc. for $C_{60}H_{46}N_6O_{18}Ni_3$: C, 54.75; H, 3.49; N, 6.39%. Found (%): C, 54.76; H, 3.50; N, 6.38%. IR (KBr pellet: cm^{-1}): 3668 (m), 3389 (s), 3075 (s), 1632 (vs), 1596 (vs), 1488 (m), 1451 (m), 1393 (s), 1260 (m), 1211 (m), 783 (m), 725 (m).

Crystallography

The X-ray single crystal data collection for complexes **1–4** was performed on a Bruker Smart Apex II CCD diffractometer equipped with graphite monochromated Mo Kα radiation (λ = 0.71073 Å) at 293(2) K. Absorption corrections were applied using the program SADABS. The structures were solved by direct methods and refined by a full matrix least squares method on F^2 using SHELXS 97 and SHELXL 97 programs.[43,44] The hydrogen atoms were generated geometrically and treated by a mixture of independent and constrained refinement. The crystallographic data are summarized in Table 1, while selected bond lengths and angles are given in Table S1.† More details of the crystal structures could be known from the Cambridge Crystallographic Data Centre.

Results and discussion

Structural description of complexes

Structure of 1. X-ray diffraction study reveals that complex **1** crystallizes in the triclinic $P\bar{1}$ space group and has a 3D

Table 1 Crystallographic data of **1–4**

Complex	**1**	**2**	**3**	**4**
Empirical formula	$C_{19}H_{14}N_3O_8Cu_2$	$C_{50}H_{30}N_4O_{14}Cu_3$	$C_{27}H_{22}N_2O_{11}Ni_2$	$C_{60}H_{46}N_6O_{18}Ni_3$
Formula weight	539.41	1101.4	667.89	1315.16
Crystal system	Triclinic	Triclinic	Triclinic	Triclinic
Space group	$P\bar{1}$	$P\bar{1}$	$P\bar{1}$	$P\bar{1}$
a (Å)	9.5272(4)	10.0683(8)	11.1024(8)	8.034(2)
b (Å)	10.6671(5)	10.8967(9)	11.5542(9)	9.981(2)
c (Å)	11.6450(5)	11.0913(9)	12.4520(9)	18.072(4)
α (°)	100.8070(10)	89.393(3)	72.963(2)	87.730(8)
β (°)	98.5420(10)	85.366(2)	72.622(2)	83.662(8)
γ (°)	115.0540(10)	64.932(2)	67.195(2)	76.257(8)
Volume (Å^3)	1017.95(8)	1098.24(15)	1376.45(18)	1398.9(5)
Z	2	1	2	1
Calculated density/Mg m^{-3}	1.760	1.665	1.611	1.561
Absorption coefficient/mm^{-1}	2.143	1.518	1.433	1.082
F(000)	542	557	684	676
Crystal size/mm^3	0.176 × 0.116 × 0.114	0.268 × 0.103 × 0.054	0.347 × 0.313 × 0.122	0.317 × 0.048 × 0.045
Theta range for data collection/(°)	3.03 to 25.01	3.02 to 25.01	2.95 to 25.01	2.95 to 25.01
Limiting indices	$-11 \le h \le 11$ $-12 \le k \le 12$ $-13 \le l \le 13$	$-11 \le h \le 11$ $-12 \le k \le 12$ $-13 \le l \le 13$	$-13 \le h \le 13$ $-13 \le k \le 13$ $-14 \le l \le 14$	$-9 \le h \le 9$ $-11 \le k \le 11$ $-21 \le l \le 21$
Reflections collected/unique	18 268/3582 [R(int) = 0.0741]	19 635/3866 [R(int) = 0.0765]	23 992/4836 [R(int) = 0.0713]	24 796/4929 [R(int) = 0.1398]
Data/restraints/parameters	3582/20/297	3866/0/322	4836/27/390	4929/7/398
Goodness-of-fit on F^2	1.032	1.022	1.047	0.996
Final R indices [$I > 2\sigma(I)$]	$R_1 = 0.0355$, w$R_2 = 0.0901$	$R_1 = 0.0403$ w$R_2 = 0.0919$	$R_1 = 0.0355$ w$R_2 = 0.0955$	$R_1 = 0.0560$ w$R_2 = 0.0921$
R Indices (all data)	$R_1 = 0.0473$ w$R_2 = 0.0966$	$R_1 = 0.0578$ w$R_2 = 0.1000$	$R_1 = 0.0388$ w$R_2 = 0.1016$	$R_1 = 0.1268$ w$R_2 = 0.1124$
Largest diff. peak and hole/e Å^{-3}	1.191 and −0.528	0.465 and −0.444	0.670 and −0.453	0.448 and −0.498

framework structure. It can be seen from Fig. 1a that the asymmetric unit consists of two crystallographically independent Cu(II) ions, one O-cpia ligand, half a btb ligand and a hydroxide ion. The copper center is in the five-coordinated geometry of CuO_4N for Cu1 and CuO_5 for Cu2, forming a square-pyramidal environment. Cu1 atom is coordinated with three oxygen atoms (O7B, O3C, O6D) from three O-cpia ligands, one oxygen atom (O2) from the hydroxide ion and one nitrogen atom (N7) from a btb ligand. The Cu1–O bond lengths are in the range of 1.949(2) to 2.128(3) Å while the bond angles of O–Cu–O/N are in the range of 84.37(11)° to 172.00(11)°. Cu2 is completed by three oxygen atoms (O1A, O4C, O8) from O-cpia ligands, and two oxygen atoms from hydroxide ions(O2, O2B) with the Cu–O distances ranging from 1.944(2) to 2.135(2) Å and the bond angles of O–Cu2–O ranging from 84.38(10)° to 175.13(11)°. The OH group as 3-connected node (μ_3-OH) connects the Cu atoms to generate a tetranuclear cluster [$Cu_4(\mu_3\text{-}OH)_2$], which is in the shape of a chair (Fig. 1b). In the tetranuclear unit, the four Cu(II) atoms are coplanar while the distance of Cu1–Cu2 is 3.4461(7) Å, Cu2–Cu2 is 3.0405(5) Å, and Cu1–Cu1 is 6.038 Å. In **1**, the O-cpia acting as a μ_6-bridging ligand adopts μ_2:$\eta^1\eta^1$/μ_2:$\eta^1\eta^1$/μ_2:$\eta^1\eta^1$ coordination mode and links six Cu atoms. As shown in Fig. 1c, each O-cpia bridges three tetranuclear [$Cu_4(\mu_3\text{-}OH)_2$] units in turn and each [$Cu_4(\mu_3\text{-}OH)_2$] unit is connected to six surrounding units and expands infinitely into the Cu–O-cpia network (Fig. 1d). The btb ligand adopts the TTT conformation with bidentate coordination mode to link Cu1 atoms to

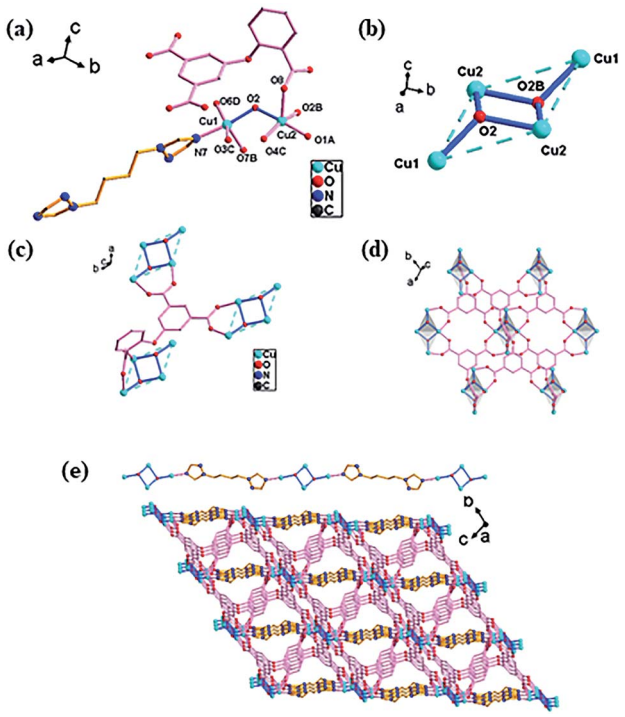

Fig. 1 Structure of **1**: (a) the coordination environment of Cu(II), (b) [$Cu_4(\mu_3\text{-}OH)_2$] cluster, (c) the coordination mode of the O-cpia ligand, (d) the Cu–O-cpia network, (e) the 3D framework. All hydrogen atoms are omitted for clarity.

form a Cu1-btb chain. Thus, the $[Cu_4(\mu_3\text{-}OH)_2]$ units as SBUs, which are bridged by O-cpia and btb mixture ligands, finally resulting in a 3D framework (Fig. 1e).

Structure of 2. As described in Fig. 2, complex **2** is also in a 3D structure, which belongs to the triclinic $P\bar{1}$ space group with one asymmetric unit containing two crystallographically independent Cu(II) atoms (CuO_3N_2 for Cu1, CuO_4 for Cu2), one O-cpia ligand and one bpy ligand. Cu1 is five-coordinated with three oxygen atoms (O2B, O5D, O7) from O-cpia ligands, and two nitrogen atoms (N1 and N2) of bpy ligand, forming a square-pyramidal geometry. Cu2 is four-coordinated with four O atoms (O1B, O1C, O6, O6E) from four O-cpia ligands in a planar quadrilateral configuration, while the angles of O–Cu2–O are 180.00(19)°, 90.16(13)°, 89.84(13)°, 89.84(13)°, 90.16(13)° and 180.00(16)° (Fig. 2a). The Cu–O/N bond lengths are comparable to those in **1**, that the bond lengths of Cu–O are in the range of 1.906(2)–2.252(2) Å, and the bond lengths of Cu–N are 1.993(2) and 2.036(3) Å. The difference is in **2**, the O-cpia adopts $\mu_2{:}\eta^1\eta^1/\mu_1{:}\eta^1\eta^0/\mu_2{:}\eta^1\eta^1$ coordination mode as a μ_5-bridging ligand linking five Cu(II) atoms, which can be seen in Fig. 2b. The adjacent three Cu atoms (Cu1, Cu2 and Cu1) are connected by COO groups, forming a trinuclear clusters $[Cu_3(COO)_4]$ with the Cu1–Cu2 distance of 3.6636(5) Å. The $[Cu_3(COO)_4]$ clusters as SUBs are connected by O-cpia ligands to Cu–O-cpia network parallel to the ab plane (Fig. 2c). The bpy ligand adopts bidentate coordination mode and links Cu1 atom, forming a Cu1-bpy chain with the Cu1–Cu1 distance of 11.0913(10) Å along the *a* axis. As shown in Fig. 2d, the Cu–O-cpia network interweave with Cu1-bpy chains, while the trinuclear clusters $[Cu_3(COO)_4]$ act as SBUs, forming a 3D framework.

Structure of 3. Different from complexes **1** and **2**, complex **3** exhibits a 2D structure with two crystallographically independent Ni(II) atoms, one O-cpia anion, a phen, one water molecule and a hydroxide ion in one asymmetric unit, as shown in Fig. 3. The Ni(II) atoms have slightly distorted octahedral coordination geometries, such as NiO_4N_2 for Ni1 and NiO_6 for Ni2. The Ni1 atom is surrounded by three carboxylate oxygen atoms (O2A, O4C and O6) from three O-cpia ligands, one oxygen atom (O8) from hydroxy and two nitrogen atoms (N1, N2) from chelating phen ligand. The bond lengths of Ni1–O are in the range of 2.0482(18)-2.0817(18) Å, while the bond lengths of Ni–N are 2.121(2) and 2.074(2) Å. The bond angles of O–Ni1–O are from 87.70(8)° to 171.01(8)°. The Ni2 atom is coordinated by three carboxylate oxygen atoms from three O-cpia (O3B, O1A and O7), two μ_3-OH (O8 and O8D) and one water molecule with the Ni–O distances ranging from 2.0561(18) to 2.1415(19) Å and the bond angles of O–Ni2–O from 84.21(7)° to 177.74(7)°, as can be seen in Fig. 3a. Similar to **1**, the adjacent Ni(II) ions are connected by

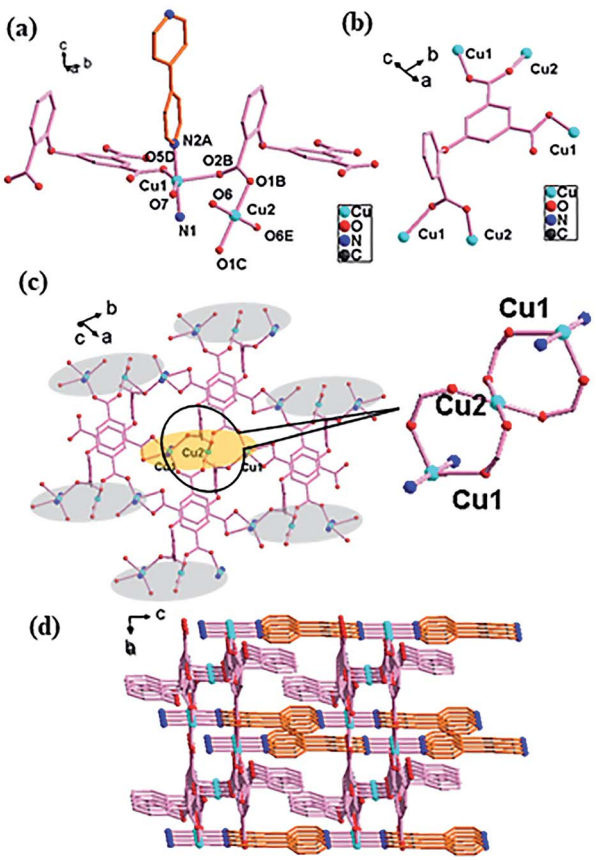

Fig. 2 Structure of **2**: (a) the coordination environment of Cu(II), (b) the coordination mode of the O-cpia ligand, (c) Cu–O-cpia network and the trinuclear clusters $[Cu_3(COO)_4]$, (d) the 3D framework. All hydrogen atoms are omitted for clarity.

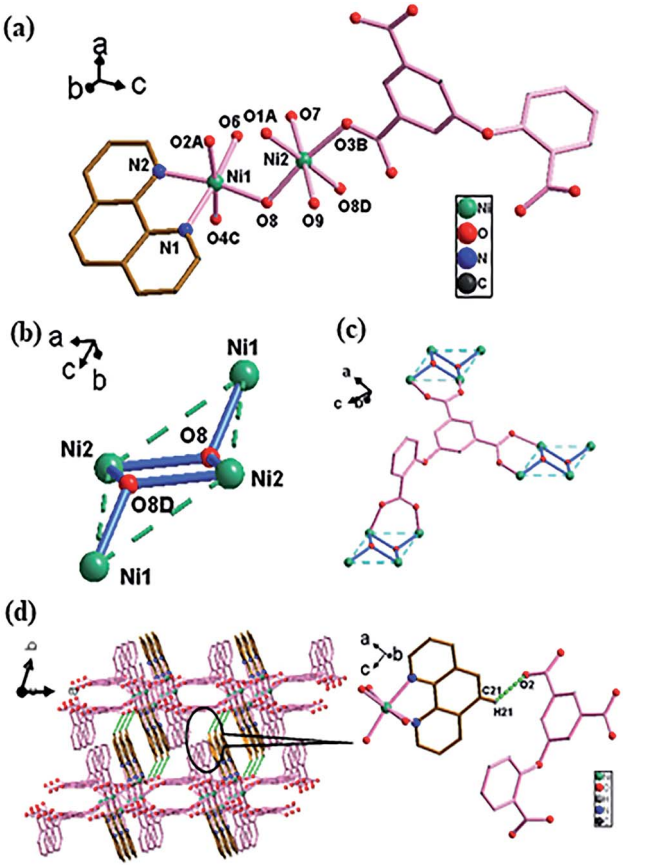

Fig. 3 Structure of **3**: (a) the coordination environment of Ni(II), (b) $[Ni_4(\mu_3\text{-}OH)_2]$ tetranuclear cluster, (c) the coordination mode of the O-cpia ligand, (d) 3D structure constructed by hydrogen bonds. All hydrogen atoms are omitted for clarity.

μ_3-OH groups, forming a $[Ni_4(\mu_3\text{-}OH)_2]$ tetranuclear cluster with the distance d(Ni1–Ni2) of 3.539(7) Å, d(Ni2–Ni2) of 3.109 Å, and d(Ni1–Ni1) of 6.194 Å (Fig. 3b). The $[Ni_4(\mu_3\text{-}OH)_2]$ clusters as SUBs are further assembled to form a 2D network by the μ_6-bridging O-cpia ligand with $\mu_2{:}\eta^1\eta^1/\mu_2{:}\eta^1\eta^1/\mu_2{:}\eta^1\eta^1$ coordination mode (Fig. 3c). The steric effect of phen probably hinders the formation of the three-dimensional (3D) structure and leads to a 2D form. In the 2D structure, each O-cpia ligand connects three $[Ni_4(\mu_3\text{-}OH)_2]$ clusters and each $[Ni_4(\mu_3\text{-}OH)_2]$ cluster is connected with six O-cpia ligands. Moreover, as illustrated in Fig. 3d, the 2D layers are assembled into a 3D supramolecular network through C–H···O hydrogen bonds (d(C···O) = 3.4066 Å) between phen and O-cpia ligands. Free water molecules fill in the structure by hydrogen bonds.

Structure of 4. Complex **4** exhibits a 3D structure, which belongs to $P\bar{1}$ space group (Fig. 4). There are two crystallographically independent Ni(II) atoms (NiO_4N for Ni1 and NiO_4N_2 for Ni2) in an asymmetric unit, with one O-cpia ligand, one and a half of bpy ligands, one coordinated water molecule and free water molecules. The Ni1 is surrounded by four oxygen atoms (O1A, O2B, O6D and O7) from four O-cpia ligands and one nitrogen atom (N1) of one bpy ligand, forming a square-pyramidal geometry. The Ni2 is attached with two oxygen atoms (O4, O4C) from two O-cpia ligands, two oxygen atoms (O8, O8C) from coordinated water molecules, and two nitrogen atoms (N3, N3C) of 4,4′-bpy ligands, forming a octahedral geometries (Fig. 4a). The Ni–O/N bond lengths are similar to that in **3**, with the bond lengths of Ni–O in the range of 1.997(3)–2.084(3) Å and the lengths of Ni–N in the range of 2.012(3)–2.070(4) Å. The bond angles of O–Ni–O/N are between 88.04(14)° and 167.36(12)°. As shown in Fig. 4b, the O-cpia acts as μ_5-bridging ligand in $\mu_2{:}\eta^1\eta^1/\mu_2{:}\eta^1\eta^1/\mu_1{:}\eta^1\eta^0$ coordination mode, linking five Ni atoms to form Ni–O-cpia network (Fig. 4c). The two adjacent Ni1 atoms are connected by COO groups, forming a binuclear cluster $[Ni_2(COO)_4]$ with the Ni1–Ni1 distance of 2.6602(12) Å. Different from complex **2**, in **4**, bpy ligands adopt two kinds of coordination modes. One bpy as terminal ligand coordinates with Ni1 atom by its one N atom, the other bpy as bidentate-bridging ligand connects two Ni2 atoms by its two N atoms to form Ni2-bpy chain with the Ni2–Ni2 distance of 11.2279 Å along a axis. The two kinds of bpy ligands are almost perpendicular. Thus, a 3D architecture, as shown in Fig. 4d, is built by the bpy ligands between Ni–O-cpia networks, in which the $[Ni_2(COO)_4]$ binuclear clusters and mononuclear metal Ni2 cores act as SUBs.

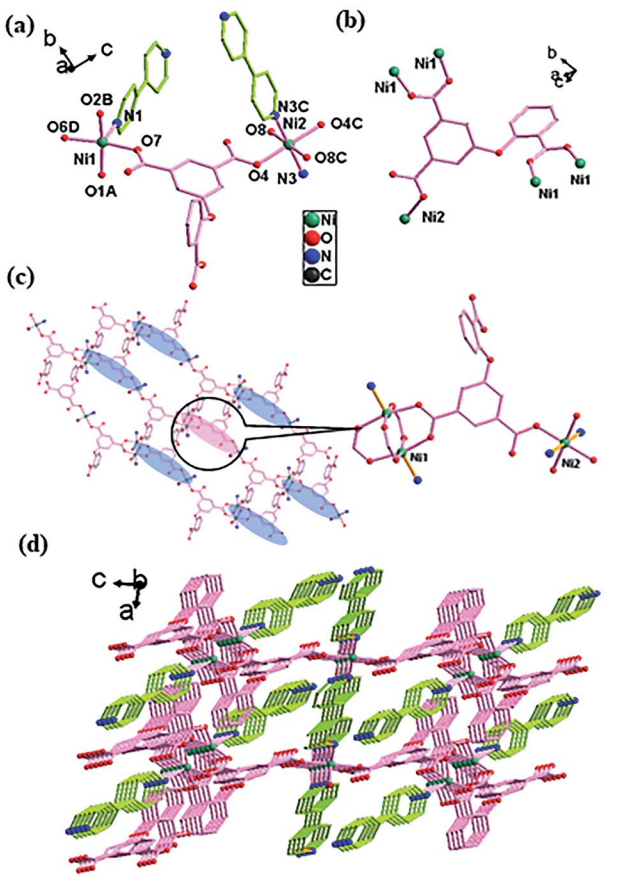

Fig. 4 Structure of **4**: (a) the coordination environment of Ni(II), (b) the coordination mode of the O-cpia ligand, (c) Ni–O-cpia network, (d) the 3D network. All hydrogen atoms are omitted for clarity.

Power X-ray diffraction (PXRD) and thermal analysis

In order to confirm the phase purity, these complexes were checked by PXRD analysis. It can be seen that experimental PXRD patterns agree with the simulated PXRD result very well. The result indicates that pure crystals have been successfully synthesized (Fig. S1†). To examine the thermal stabilities of the complexes, thermogravimetric analysis (TGA) were employed at a heating rate of 10 °C min^{-1} in air atmosphere. The results are shown in Fig. S2.† It can be seen that complexes **1** and **2** are stable up to 282 and 320 °C, respectively. With the increase of temperature, the organic ligands in the complexes decomposed. The residue can be attributed to CuO (for **1**, calcd: 70.2%, found: 69.6%; for **2**, calcd: 78.3%, found: 78.1%). For complex **3**, a weight loss of 8.5% is observed from 51 to 172 °C, while for **3**, a weight loss of 4.4% is observed between 58 and 201 °C. The weight loss can be attributed to the loss of the coordinated water molecules and lattice water molecules (calcd 8.1% for **3** and 5.4% for **4**). The skeleton began to collapse at 299 °C for **3** and 324 °C for **4**, and the residue may be NiO (calcd: 77.0%, found: 82.0% for **3** and calcd: 83.0%, found: 84.1% for **4**).

Photocatalytic activities

To explore the photocatalytic potential of the compounds, the solid UV diffuse reflectance spectra of the complexes were recorded at room temperature, as shown in Fig. 5. The spectra of these compounds show different absorption activities in the visible region from 200 to 800 nm. According to the equation $(\alpha h\nu = K(h\nu - E_g)^{1/n}$, where α is the absorption coefficient, $h\nu$ is the discrete photo energy, K is a constant, E_g is the band gap energy, n equals 1/2 for indirect transition), the extrapolated values of $h\nu$ at $\alpha = 0$ give absorption edge energies (E_g) of complexes.[45–47] The absorption edge energies are 1.30 eV for **1** and 1.78 eV for **2**, which are lower than those for **3** (2.85 eV) and **4** (2.14 eV) in Fig. S3.† The band gap sizes of **1–4** indicate that they may have potential capacity for photocatalytic reactions.

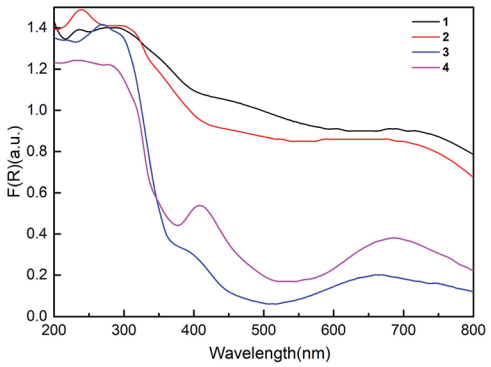

Fig. 5 The solid state UV-vis reflectance spectra of compounds **1**, **2**, **3** and **4**.

In recent years, coordination polymers, as a kind of photocatalyst, have attracted much attention due to their potential applications in purifying waste water under visible light irradiation by decomposing organic dyes. To study the photocatalytic activity of the complexes as catalysts, rhodamine B (RhB) was selected as a representative dye, and the test was carried under visible light illumination. For this experiment, 30 mg compound and 500 mL RhB (1.0×10^{-5} mol L^{-1}) were mixed and stirred for half an hour to achieve the equilibrium condition in the dark environment. Then, 4 mL H_2O_2 was added under visible light irradiation at a temperature of 298.15 K. Equivalent samples from the reaction system were taken for the measurement every 10 min, and the degradation progress was monitored by observing the intensity of the characteristic absorption band of RhB at 553 nm. Blank experiments in the presence of H_2O_2 and the absence of the photocatalyst were also performed.

As can be seen in Fig. S4,† with the presence of compound only, the concentration of RhB shows very little reduction after 1.5 h, which is 4.2% (for **1**), 4.6% (for **2**), 3.6% (for **3**) and 6.0% (for **4**), respectively. Compared with the presence of compound and H_2O_2, different results for degradation was observed in the case of the complexes, as shown in Fig. 6. When using an equimolar amount of **1** as the catalyst for degradation of dichromate under the same conditions, 28%, 52%, 80% and 88% reduction of RhB were observed after 20, 40, 70 and 90 min, respectively. Similarly, when using **2** as the catalyst, 25%, 48%, 73% and 81% of RhB were degradated after 20, 40, 70 and 90 min, respectively. However, **3** and **4** have low photocatalytic efficiency. In the same time of 1.5 h, about 5.0% RhB (for 20 min), 9.0% (for 40 min), 19% (for 70 min) and 23% (for 90 min) are decomposed under visible light irradiation when **3** used as the catalyst. For **4**, about 6.0% RhB (for 20 min), 11% (for 40 min), 20% (for 70 min) and 26% (for 90 min) are decomposed. The results indicate that **1** and **2** possess better photocatalytic efficiency than **3** and **4**, as shown in Fig. 7.

In addition, the blank experiments of the degradation of organic pollutants were finished in the same reaction condition without using the addition of compound. As shown in Fig. 8, in the presence of only H_2O_2, the degradation of RhB are merely 23% after 90 min under visible light irradiation.

The photocatalytic behaviors of **1**–**4** for the degradation of RhB under visible light irradiation are summarized in Fig. 9. As can be seen, the catalytic efficiency for the degradation of RhB is **1** > **2** > **4** > **3**. Interestingly, the order is opposite to that of their

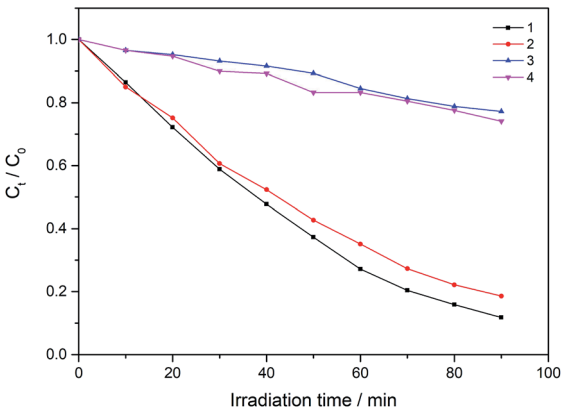

Fig. 7 Change of absorption spectra of the solution of RhB with H_2O_2 and different complexes under visible light irradiation. C_t and C_0 stand for the RhB concentrations after and before irradiation.

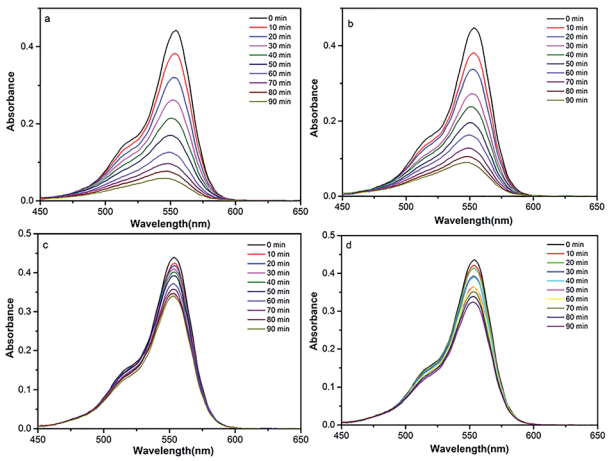

Fig. 6 Absorption spectra of RhB degraded with complex and H_2O_2 (**1** (a), **2** (b), **3** (c) and **4** (d)) under visible light illumination.

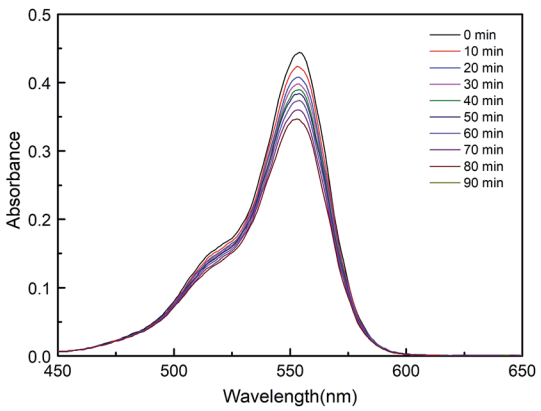

Fig. 8 Absorption spectra of the solution of RhB with H_2O_2 under visible light irradiation.

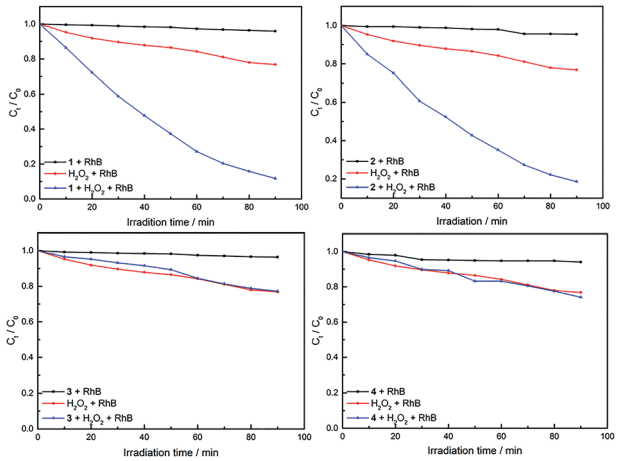

Fig. 9 RhB degradation profile under different conditions: (black) visible light with the presence of MOFs, (red) visible light with the presence of H_2O_2, (blue) visible light with the presence of H_2O_2 and MOFs. C_t and C_0 stand for the RhB concentrations after and before irradiation.

Eg (**3** > **4** > **2** > **1**). The similar relationship of E_g and catalytic rate has been reported previously.[48] These results indicate that the Cu(II) complexes have a faster degradation rate for the RhB than the Ni(II) complex, which can be attributed to the nature of the metal cation used, that Cu(II) is a more active metal cation than Ni(II).[49] Meanwhile, Cu(II) and Ni(II) have different electronic configurations and geometries, which may also influence the photocatalytic activity.[50,51] In addition, based on the good catalytic performance of complexes **1–2**, the catalytic performance of **1–2** for methylene blue (MB) and methyl orange (MO) was measured. The experimental results are shown in Fig. S5–S8.† When complexes **1** and **2** used as the catalyst, respectively, the 94% MB/61% MO and 89% MB/42% MO (90 min) were decomposed under visible light irradiation.

The reaction mechanism for dyes photodegradation has been discussed based on semiconductor theory.[26,48,49,52] When the complex is irradiated by a xenon lamp, the electrons in the valence band are easily excited into the conduction band, which increases the amount of holes (h^+) in the valence band. Then electrons may combine with O_2 on the surface of the complex to form oxygen radical, which will further produce hydroxyl free (·OH). Meanwhile, hydrogen peroxide itself could also decompose to generate oxygen (O_2) and hydroxide (OH^-), the O_2 and OH^- present in the solution are adsorbed on the surface of the complex. At the same time, (OH^-) adsorpted on the surface of the complex interacts with holes (h^+), generating (·OH). As the most effective group for catalytically degrading organic dyes, (·OH) can degrade organic dyes into inorganic ions. Therefore, the synergistic catalysis of complexes **1**, **2** and hydrogen peroxide improves the efficiency of photocatalytic degradation of RhB.

Four complexes derived from O-cpia, Cu(II)/Ni(II) and various co-N-ligands show several interesting structural features. In the frameworks, the tetranuclear clusters [$Cu_4(\mu_3$-$OH)_2$] and [$Ni_4(\mu_3$-$OH)_2$] (in **1** and **3**), trinuclear cluster [$Cu_3(COO)_4$] (in **2**), and the binuclear unit [$Ni_2(COO)_4$]/mononuclear metal (Ni2) unit (in **4**) are found, which act as SBUs to be assembled into different framework structures by O-cpia and co-N-ligands. Moreover, each asymmetric unit contains two crystallographically independent metal(II) center atoms with different metal polyhedra. Ni(II) forms a the octahedral coordination geometry while Cu(II) forms square-pyramidal or planar quadrilateral geometry due to the larger radius of Ni(II) than that of Cu(II). O-cpia ligand exhibits different bridging coordination modes and acts as μ_6-bridging (in **1** and **3**) and μ_5-bridging (in **2** and **4**) ligand, respectively, while N-ligands, phen, bpy and btb are used to tune the dimensionality of the complexes. The bpy and btb ligands have bridging function to form high dimensional architectures (3D, **1**, **2** and **4**). When the terminal ligand phen is introduced into the system, the resulting complex **3** shows a 2D network structure. The auxiliary N-ligands play an important role in governing the formation of the final frameworks. Meanwhile, the degradation of RhB by the complexes under visible light irradiation were studied. **1–4** are semiconducting in nature, with Eg of 1.30 eV (**1**), 1.78 eV (**2**), 2.85 eV (**3**) and 2.14 eV (**4**). **1–2** are universal and highly efficient photocatalysts for the degradation of RhB under visible light irradiation. They are stable and can be easily separated from the reaction system for reuse. Photocatalytic activity of Cu(II) and Ni(II) complexes against dyes under visible light irradiation were studied and the Cu(II) complexes (**1–2**) exhibit a higher photocatalysts activity than the Ni(II) complexes (**3–4**).

Conclusions

In summary, four metal–organic frameworks, namely, Cu_2(O-cpia)$(btb)_{0.5}\cdot(OH)$ (**1**), Cu_3(O-cpia)$_2(bpy)_2$ (**2**), [Ni_2(O-cpia)$(phen)\cdot(OH)\cdot H_2O]\cdot 2H_2O$ (**3**) and [Ni_3(O-cpia)$_2(bpy)_3\cdot 2H_2O]\cdot 2H_2O$ (**4**) were synthesized through hydrothermal reactions. Compounds **1**, **2**, and **4** possess different complicated 3D frameworks whereas **3** exhibits a 2D structure. They display different homometallic clusters varying from mononuclear, binuclear to tetranuclear metal(II) units as SBUs within the frameworks. O-cpia ligand exhibits bridging coordination modes for coordination polymer structure, while the structural characteristics of auxiliary N-ligands also play an important role in governing the structures of such complexes. **1** and **2** are universal and more efficient photocatalysts than **3** and **4** for the degradation of RhB under visible light irradiation. This work provides new information regarding polynuclear metal(II) chemistry and the MOFs prepared in this paper can be applied to the degradation of organic dye.

Conflicts of interest

There are no conflicts to declare.

Acknowledgements

The authors are grateful to the Key Project of Science and Technology plan of Beijing Education Commission (KZ201910028038) and the National Natural Science Foundation of China (21471104).

Notes and references

1 Z. J. Lin, J. Lv, M. Hong and R. Cao, *Chem. Soc. Rev.*, 2014, **43**, 5867–5895.
2 G. Maurin, C. Serre, A. Cooper and G. Ferey, *Chem. Soc. Rev.*, 2017, **46**, 3104–3107.
3 J. Poater, M. Gimferrer and A. Poater, *Inorg. Chem.*, 2018, **57**, 6981–6990.
4 H. C. Zhou and S. Kitagawa, *Chem. Soc. Rev.*, 2014, **43**, 5415–5418.
5 N. Stock and S. Biswas, *Chem. Rev.*, 2012, **112**, 933–969.
6 S. Seth, G. Savitha and J. N. Moorthy, *Cryst. Growth Des.*, 2018, **18**, 2129–2137.
7 G. Mínguez Espallargas and E. Coronado, *Chem. Soc. Rev.*, 2018, **47**, 533–557.
8 Y. Wang, M. He, X. Gao, Y. Zhang, H. Zhong, P. Long, X. Wang and Y. He, *Inorg. Chem. Front.*, 2018, **5**, 2811–2817.
9 J. Yu, L. H. Xie, J. R. Li, Y. Ma, J. M. Seminario and P. B. Balbuena, *Chem. Rev.*, 2017, **117**, 9674–9754.
10 E. A. Dolgopolova, A. M. Rice, C. R. Martin and N. B. Shustova, *Chem. Soc. Rev.*, 2018, **47**, 4710–4728.
11 M. C. Bernini, A. E. Platero-Prats, N. Snejko, E. Gutiérrez-Puebla, A. Labrador, R. Sáez-Puche, J. Romero de Paz and M. A. Monge, *CrystEngComm*, 2012, **14**, 5493.
12 X.-L. Qu, X.-L. Zheng and X. Li, *RSC Adv.*, 2016, **6**, 69007–69015.
13 T. Devic and C. Serre, *Chem. Soc. Rev.*, 2014, **43**, 6097–6115.
14 Y. Q. Sun, J. C. Zhong, L. Ding and Y. P. Chen, *Dalton Trans.*, 2015, **44**, 11852–11859.
15 Y. Qiao, Y. Ma, W. Jiang, X. Wang, W. Guan, G. Che, W. Li and F. Qin, *CrystEngComm*, 2018, **20**, 7782–7794.
16 Z. J. Wang, L. J. Han, X. J. Gao and H. G. Zheng, *Inorg. Chem.*, 2018, **57**, 5232–5239.
17 Z. Li, J. Guo, F. Xiang, Q. Lin, Y. Ye, J. Zhang, S. Chen, Z. Zhang and S. Xiang, *CrystEngComm*, 2018, **20**, 7567–7573.
18 F. Wan, L. X. Qiu, L. L. Zhou, Y. Q. Sun and Y. You, *Dalton Trans.*, 2015, **44**, 18320–18323.
19 N. Ahmad, H. A. Younus, A. H. Chughtai, K. Van Hecke, Z. A. K. Khattak, Z. Gaoke, M. Danish and F. Verpoort, *Catal. Sci. Technol.*, 2018, **8**, 4010–4017.
20 R. Kaur, A. Kaur, A. Umar, W. A. Anderson and S. K. Kansal, *Mater. Res. Bull.*, 2019, **109**, 124–133.
21 S. Kongchoo, K. Chainok, A. Kantacha and S. Wongnawa, *Inorg. Chem. Commun.*, 2017, **83**, 97–102.
22 S. Sanram, J. Boonmak and S. Youngme, *Polyhedron*, 2016, **119**, 151–159.
23 Y. Li, J. Jiang, Y. Fang, Z. Cao, D. Chen, N. Li, Q. Xu and J. Lu, *ACS Sustainable Chem. Eng.*, 2018, **6**, 16186–16197.
24 L. Lu, J. Wang, S.-L. Cai, B. Xie, B.-H. Li, J.-H. Man, Y.-X. He, A. Singh and A. Kumar, *J. Coord. Chem.*, 2017, **70**, 3409–3421.
25 N. Ahmad, H. A. Younus, A. H. Chughtai, K. Van Hecke, Z. A. K. Khattak, Z. Gaoke, M. Danish and F. Verpoort, *Catal. Sci. Technol.*, 2018, **8**, 4010–4017.
26 H. Chen, P. X. Liu, N. Xu, X. Meng, H. N. Wang and Z. Y. Zhou, *Dalton Trans.*, 2016, **45**, 13477–13482.
27 Y. Zhou, L. Qin, M.-K. Wu and L. Han, *Cryst. Growth Des.*, 2018, **18**, 5738–5744.
28 F. Wei, D. Chen, Z. Liang and S. Zhao, *Nanomaterials*, 2018, **8**, 248.
29 X. R. Wang, Z. Huang, J. Du, X. Z. Wang, N. Gu, X. Tian, Y. Li, Y. Y. Liu, J. Z. Huo and B. Ding, *Inorg. Chem.*, 2018, **57**, 12885–12899.
30 R. Mishra, M. Ahmad, M. R. Tripathi and R. J. Butcher, *Polyhedron*, 2013, **50**, 169–178.
31 P. Lama, J. Mrozinski and P. K. Bharadwaj, *Cryst. Growth Des.*, 2012, **12**, 3158–3168.
32 X.-m. Meng, X.-y. Zhang, X.-p. Wang, R.-x. Wu, X. Zhang, F. Jin and Y.-h. Fan, *Polyhedron*, 2017, **137**, 81–88.
33 R. Ma, Z. Chen, S. Wang, C. Zhou, Y. Li, J. Lu, D. Li and J. Dou, *Inorg. Chem. Commun.*, 2017, **81**, 59–66.
34 Ž. Zupanek, M. Tramšek, A. Kokalj and G. Tavčar, *Inorg. Chem.*, 2018, **57**, 13866–13879.
35 W. Q. Zhang, R. D. Wang, Z. B. Wu, Y. F. Kang, Y. P. Fan, X. Q. Liang, P. Liu and Y. Y. Wang, *Inorg. Chem.*, 2018, **57**, 1455–1463.
36 J. L. Zhang, J. Yang, X. Wang, H. Y. Zhang, X. L. Chi, Q. Yang, Y. Chen and D. R. Xiao, *Inorg. Chim. Acta*, 2016, **447**, 66–76.
37 J.-M. Li, R. Li and X. Li, *CrystEngComm*, 2018, **20**, 4962–4972.
38 X. Pang, L. Li, Y. Wei, X. Yu and Y. Li, *Dalton Trans.*, 2018, **47**, 11530–11538.
39 Y. Zhao, L. Wang, N.-N. Fan, M.-L. Han, G.-P. Yang and L.-F. Ma, *Cryst. Growth Des.*, 2018, **18**, 7114–7121.
40 M. B. Coban, *J. Mol. Struct.*, 2019, **1177**, 331–337.
41 X.-L. Qu, X.-L. Zheng and X. Li, *RSC Adv.*, 2016, **6**, 69007–69015.
42 M.-N. Zhang, T.-T. Fan, Q.-S. Wang, H.-L. Han and X. Li, *J. Solid State Chem.*, 2018, **258**, 744–752.
43 G. M. Sheldrick, *SHELXS-97, Program for Crystal Structure Refinement*, University of Göttingen, 1997.
44 G. M. Sheldrick, *SHELXL-97, Program for Crystal Structure Solution*, University of Göttingen, 1997.
45 W. Hu, L. Li, G. Li, C. Tang and L. Sun, *Cryst. Growth Des.*, 2009, **9**, 3676–3682.
46 Y.-S. Chang, M. Choi, M. Baek, P.-Y. Hsieh, K. Yong and Y.-J. Hsu, *Appl. Catal., B*, 2018, **225**, 379–385.
47 Y.-H. Chiu, K.-D. Chang and Y.-J. Hsu, *J. Mater. Chem. A*, 2018, **6**, 4286–4296.
48 J. Liu, Y. H. Tang, F. Wang and J. Zhang, *CrystEngComm*, 2018, **20**, 1232–1236.
49 P. M. Krishna, N. B. Reddy, N. Kottam, B. C. Yallur and H. R. Katreddi, *Sci. World J.*, 2013, 828313.
50 H. R. Mardani, A. Esmaeili and A. Malekzadeh, *Res. Chem. Intermed.*, 2018, **44**, 6183–6195.
51 X. T. Zhang, H. T. Chen, B. Li, G. Z. Liu and X. Z. Liu, *Dalton Trans.*, 2018, **47**, 1202–1213.
52 T. R. Zheng, L. L. Qian, M. Li, Z. X. Wang, K. Li, Y. Q. Zhang, B. L. Li and B. Wu, *Dalton Trans.*, 2018, **47**, 9103–9113.

